

Supplementary Materials: Preliminary Characterization of a Ni²⁺-Activated and Mycothiol-Dependent Glyoxalase I Enzyme from *Streptomyces coelicolor*

Uthaiwan Suttisansanee and John F. Honek

		1	2	3	4	5	6	7	8	9	10	11
E. coli	1		79.26	62.32	49.28	45.21	29.57	26.67	26.63	27.27	19.25	14.91
Y. pestis	2	79.26		55.80	49.28	42.47	29.03	27.18	27.72	27.97	19.88	14.29
N. meningitidis	3	62.32	55.80		57.97	42.47	33.33	30.81	31.55	27.40	21.74	13.66
P. aeruginosa GloA2	4	49.28	49.28	57.97		34.93	29.57	26.42	30.43	24.46	19.48	12.42
L. major	5	45.21	42.47	42.47	34.93		23.94	24.24	25.13	22.88	15.48	13.84
P. aeruginosa GloA3	6	29.57	29.03	33.33	29.57	23.94		49.74	52.78	21.43	16.15	10.88
H. sapiens	7	26.67	27.18	30.81	26.42	24.24	49.74		49.47	18.52	14.00	12.32
P. putida	8	26.63	27.72	31.55	30.43	25.13	52.78	49.47		19.55	16.49	12.76
B. subtilis (Ywbc)	9	27.27	27.97	27.40	24.46	22.88	21.43	18.52	19.55		20.26	13.25
PDO	10	19.25	19.88	21.74	19.48	15.48	16.15	14.00	16.49	20.26		17.71
PLA	11	14.91	14.29	13.66	12.42	13.84	10.88	12.32	12.76	13.25	17.71	

Figure S1. Percent identities calculated for various Glo1 in the sequence alignment shown in the main text (Figure 5).

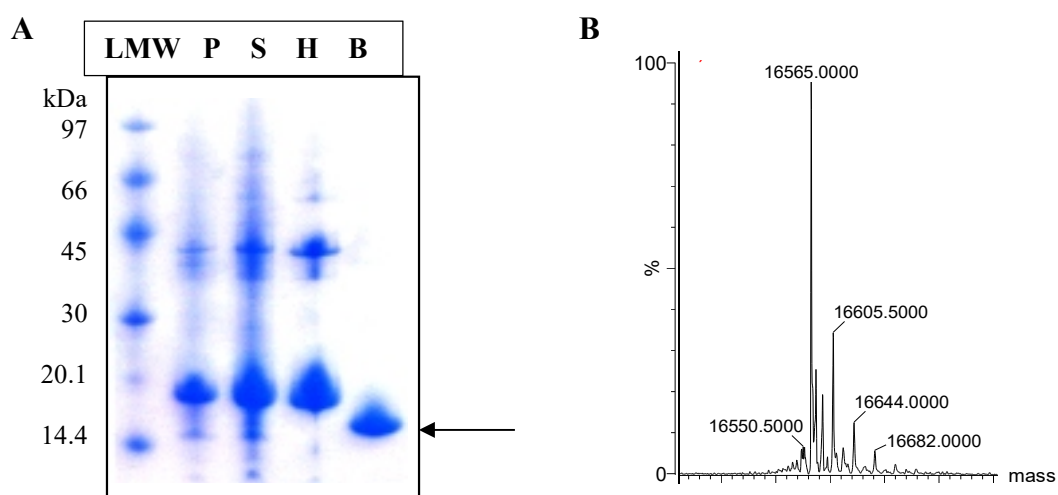


Figure S2. (A) The SDS-PAGE of the PDO purification: LMW = low molecular weight marker, P = pellet after sonication, S = supernatant after sonication, H = HisTrap eluted fraction and B = HisTrap and Benzamidine eluted fraction after thrombin protease treatment. The arrow indicates the presence of PDO. (B) The electrospray mass spectrum (% abundance versus protein mass) of PDO exhibits a molecular mass of 16565 Da (calculated MW is 16569.5 Da). Masses of 16605.5 Da and 16644 Da have been assigned as M⁺ + K⁺ and M⁺ + 2K⁺ respectively.

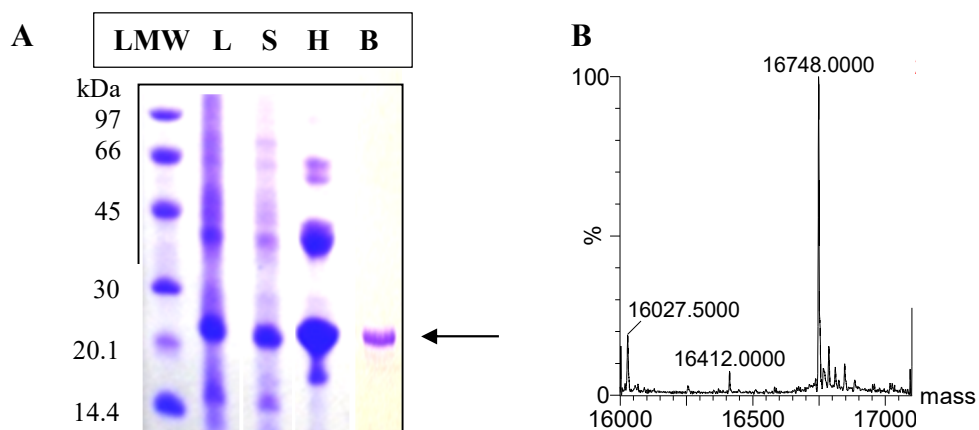


Figure S3. (A) The SDS-PAGE result of PLA purification: LMW = low molecular weight marker, L = lysate, S = supernatant after sonication, H = HisTrap fraction and B = HisTrap and Benzamidine fraction after thrombin protease treatment. The arrow indicates the presence of PLA. (B) The electrospray mass spectrum (% abundance versus protein mass) of PLA with a molecular mass of 16748.0 Da (calculated MW is 16749.9 Da).

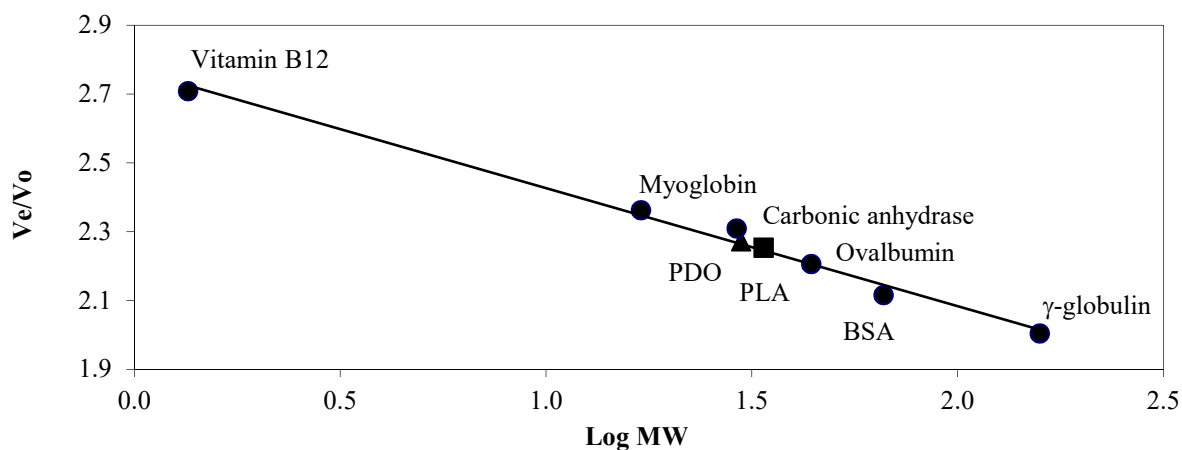


Figure S4. The gel permeation chromatographic profile of (▲) PDO (1.5 mg/mL) and (■) PLA (0.6 mg/mL) in 50 mM Tris (pH 8.0) and 150 mM KCl employing a Superose 6 10/300 GL column with 0.5 mL/min flow rate that fits onto a plot of the Bio-Rad protein standards (●) including γ -globulin (158 kDa), BSA (66 kDa), ovalbumin (44 kDa), carbonic anhydrase (29 kDa), myoglobin (17 kDa) and vitamin B12 (1.35 kDa).

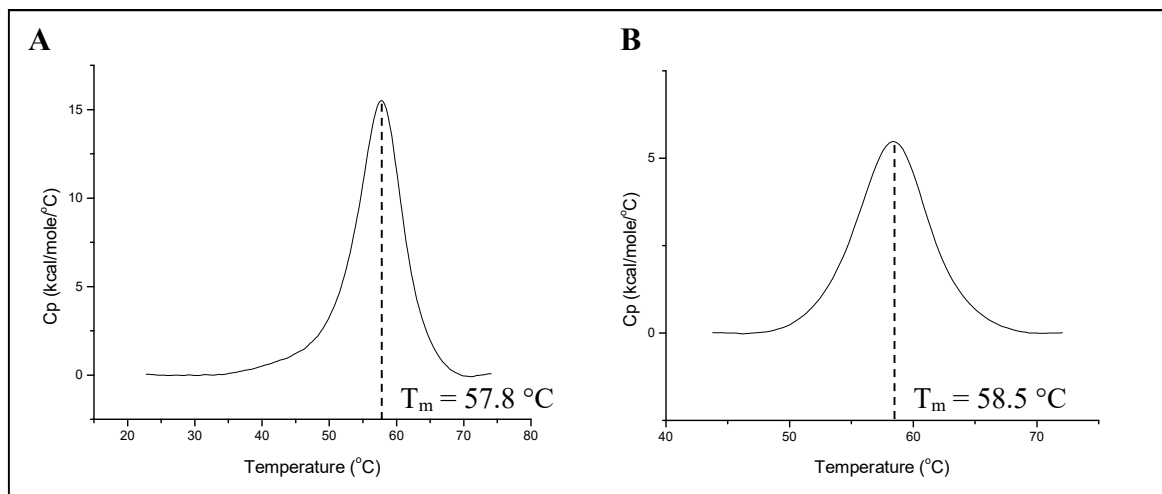


Figure S5. Heat capacity (C_p) versus temperature (T) exhibiting the temperature for the transition midpoint (T_m) of **(A)** PDO (3 mg/mL) and **(B)** PLA (1.2 mg/mL) in 50 mM MOPS (pH 7.0) and 10% (v/v) glycerol as determined by DSC analysis. The experiments were performed on a MicroCal VP-DSC microcalorimeter with cell volumes of 0.5 mL and self-contained pressurizing system of 0–30 p.s.i. for scanning solutions above boiling points to prevent any degassing during heating. The sample and the reference solutions were degassed, and the temperature was adjusted in an evacuated chamber at room temperature and carefully loaded into the cell of the calorimeter to eliminate air bubbles. The experiments with proteins were run against MOPS buffer over a temperature range of 10–80 °C with a scanning rate of 1 °C/min. Several up- and down-scans were performed for reference to obtain a stable baseline. The reference was replaced by the protein sample in the sample cell and was run using the same parameters. To test protein stability, the sample was allowed to run another round of up- and down-scans. The Origin scientific plotting software package supplied by MicroCal was used for baseline subtraction and T_m calculation by integration of the heat capacity versus temperature curve.

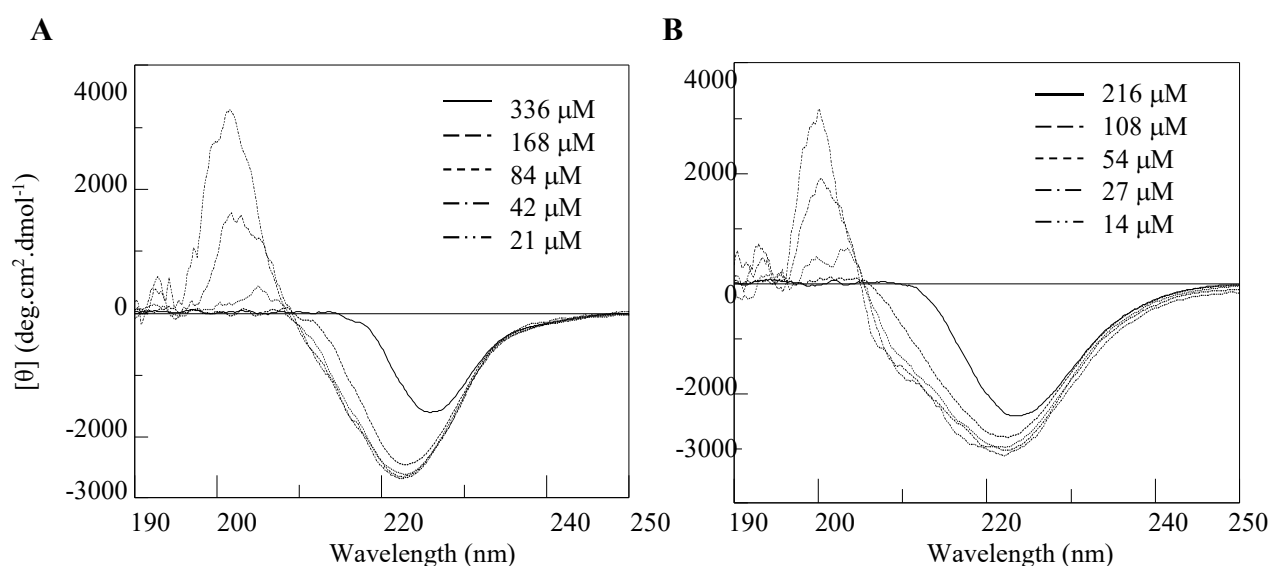


Figure S6. The CD spectra of **(A)** PDO (11.2, 5.6, 2.8, 1.4 and 0.7 mg/mL) and **(B)** PLA (7.2, 3.6, 1.8, 0.9 and 0.5 mg/mL) in buffer containing 50 mM KPB (pH 7.0) and 200 mM KCl scanning between 190–250 nm. The CD spectra of PDO at low protein concentrations (<5.6 mg/mL) possessed a negative maximum at 222 nm, a small shoulder at 211 nm and a positive band at wavelengths less than 209 nm. As the protein concentration increased (>5.6 mg/mL), the negative band at 222 nm shifted to 227 nm and the small shoulder at 211 nm became unnoticeable. The changes in shape and shift of the CD spectra suggest the possible formation of oligomers at higher concentrations. The secondary structure investigation of PLA by CD was similar to that of PDO. The CD spectra of PLA at low protein concentrations (<3.6 mg/mL) exhibited a negative maximum at 222 nm and a shoulder at 208 nm. This protein seemed to contain more β -sheet structure than PDO since it contained higher negative absorbance at 208 nm. The changes in shape and shift of the CD spectra suggest the possible formation of oligomers at higher concentrations.

Determination of Hemithioacetal Equilibrium Time

The time for the formation of the hemithioacetal substrate, MG-tMSH, to form and reach equilibrium when methylglyoxal (MG) and the synthesized truncated mycothiol, tMSH, are reacted non-enzymatically was investigated using the enzymatic assay as well as ^1H NMR. MG-tMSH (using 16 mM MG and 0.6 mM tMSH or 0.5 mM MG-tMSH initially assuming that the dissociation constant (K_a) would be similar to that of the MG-glutathione hemithioacetal, MG-GSH, which is 3.1 mM [1–6]) was incubated for various time periods over 0–3 h in 50 mM KPB (pH 6.6) at room temperature. The enzyme assay was then performed with Ni^{2+} -reconstituted PDO (apo-enzyme with additional 5 equivalents of metal, 4.5 μg in 300 μL assay) employing a 96-well UV plate using a SpectraMax spectrophotometer. The formation of the thioester product (*S*-D-lactoyl-des-*myo*-inositol mycothiol) was indicated by an increase in absorption at 240 nm assuming that this product has the same absorption as *S*-D-lactoylglutathione (the product of Glo1 reaction using GSH as cofactor) due to the presence of the common thioester moiety in both products. The equilibrium time for the formation of the MG-GSH hemithioacetal was performed in parallel by determining the enzymatic assay utilizing Glo1 (*S. cerevisiae* Glyoxalase I; Sigma Inc.) using MG-GSH (0.5 mM) in 50 mM KPB (pH 6.6) that was incubated at different time periods at room temperature.

Analysis of the activity profiles suggested that the equilibrium time for formation of the MG-GSH hemithioacetal under these conditions was 15 min, consistent with previous reports on the properties of the MG-GSH hemithioacetal (Figure S7A) [1–7]. However, a longer incubation time for the equilibrium formation of the MG-tMSH hemithioacetal was observed (30 min) (Figure S7B), suggesting that the formation of the hemithioacetal between these two substrates reaches equilibrium somewhat more slowly.

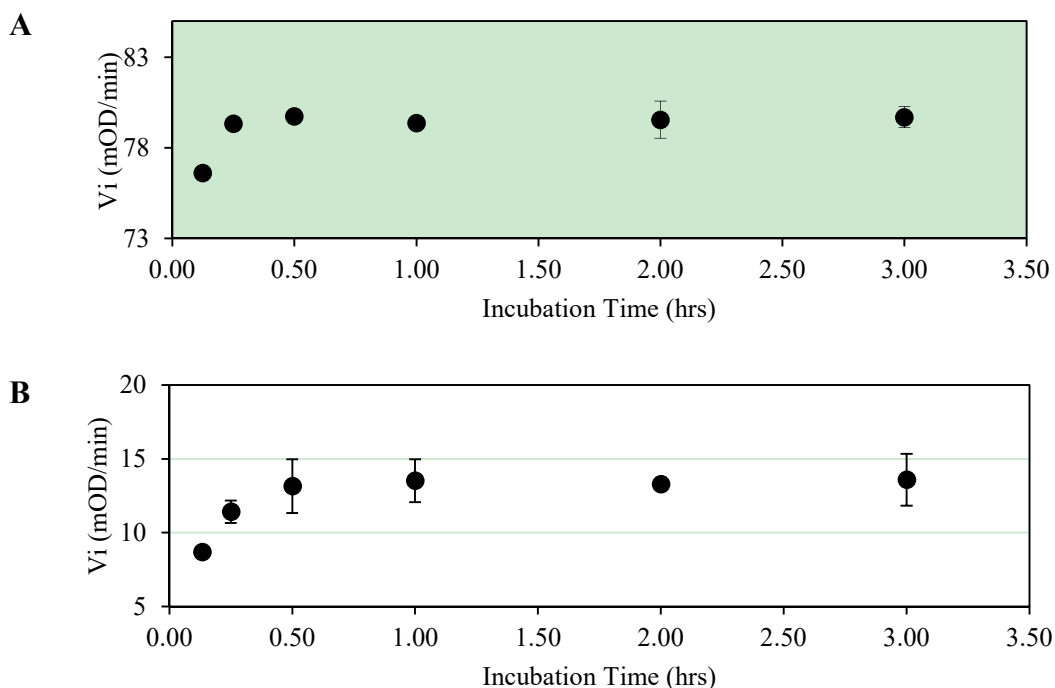


Figure S7. The enzymatic assay using various incubation times of (A) MG-GSH (0.5 mM) followed by reaction with yeast Glo1 (0.15 μ g in 300 μ L assay) and (B) MG-tMSH (0.5 mM) with Ni^{2+} -reconstituted PDO (4.5 μ g in 300 μ L assay) in 50 mM KPB (pH 6.6) at room temperature (25 $^{\circ}$ C).

In addition, 1H NMR (300 MHz) was utilized to also provide information on the equilibration time. The MG-tMSH hemithioacetal (7 mM, $K_d = 3.1$ mM) in D_2O was incubated at room temperature for different time periods, and the equilibration time was analysed using 1H NMR. Analysis of the formation of the hemithioacetal of MG-GSH (7 mM, $K_d = 3.1$ mM) in D_2O was also performed in parallel as a control (Figure S8). The resulting NMR spectra obtained for the formation of the MG-GSH were compared with the reported NMR spectrum obtained by Rae *et al.*, 1994 [8]. Alteration of several NMR resonances over time as the hemithioacetal formed were observed (Figure S8). Although various hydrates of MG complicate the 1H NMR spectra, as has been noted by Rae *et al.* [8], the resonances of the glutathione H-5 protons (region between 3.1-2.8 ppm) were clearly observed to alter over reaction time with MG. In the current experiment, the change in chemical shift of H-5 (δ 2.88–2.82 ppm in GSH and δ 3.07-2.82 in the hemithioacetal) as well as additional splitting as a result of formation of diastereomeric MG adducts is consistent with the formation of the MG-GSH hemithioacetal. No significant change in NMR signals were observed after 15 min incubation, thus consistent with the previous investigation using the literature enzymatic assay.

Table S1 summarizes calculated versus experimental chemical shifts for GSH and the MG-GSH hemithioacetal. The estimated chemical shifts were calculated employing ChemBioDraw Ultra 12.0 software (<http://www.cambridgesoft.com>).

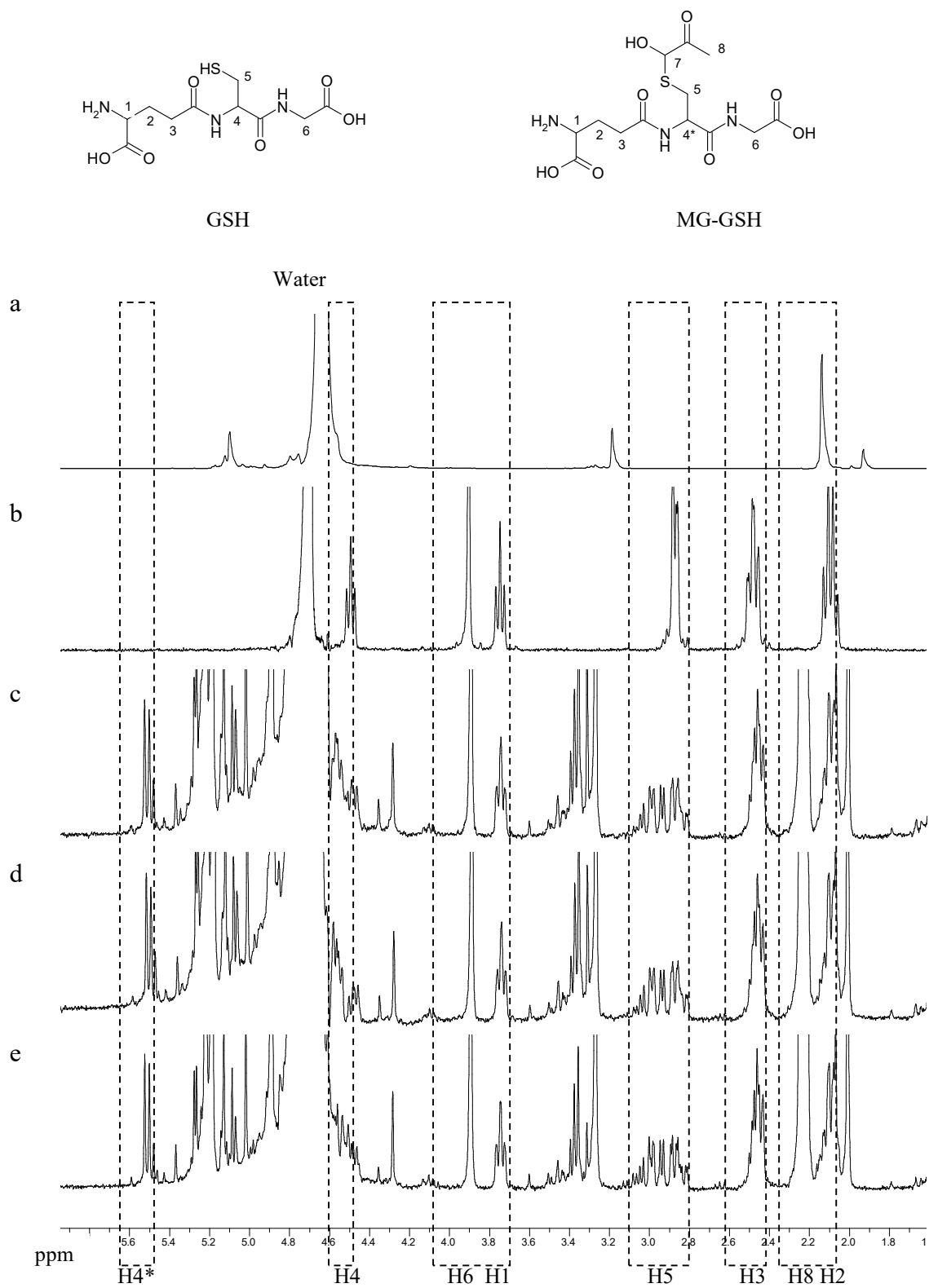
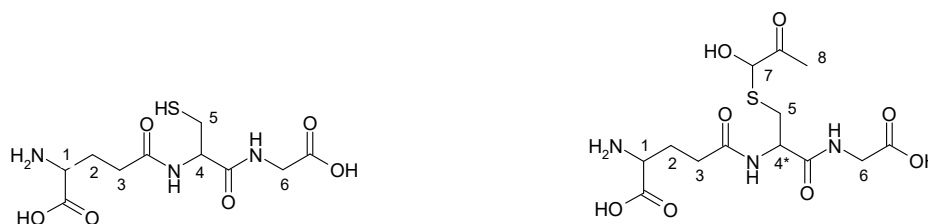


Figure S8. The ^1H NMR (300 MHz) spectra for various incubation times for the formation of the hemithioacetal of MG-GSH: (a) MG, (b) GSH, (c) reaction incubated for 8 min, (d) reaction incubated for 15 min and (e) reaction incubated for 30 min. .

Table S1. Summary of chemical shifts (CS) and integrations (int.) of NMR signals for the MG-GSH equilibration time experiments compared to the resonances for GSH.

Peak	GSH				MG-GSH			
	[†] Predicted CS (ppm)	Actual CS (ppm)	Predicted int.	Actual int.	[†] Predicted CS (ppm)	Actual Cs (ppm)	Predict Int.	Actual int.
H1	4.06	3.75	1	1.01	2.89	3.75	1	0.86
H2	2.23	2.09	2	2.25	1.75–1.96	2.18–2.05	2	2.79
H3	2.60	2.49	2	2.16	2.35	2.47	2	2.03
H4	4.01	4.49	1	1.03	5.62	5.51	1	1.24
H5	2.94	2.88	2	2.12	3.21	3.07–2.80	2	1.79
H6	4.03	3.91	2	2.19	4.13	3.91	2	2.02
H7	-	-	-	-	4.39	-	1	-
H8	-	-	-	-	2.19	2.26	3	4.42

[†]Chemical shifts were estimated by ChemBioDraw Ultra 12.0 (<http://www.cambridgesoft.com>) software.

Similar to the detection of the MG-GSH hemithioacetal adduct, the NMR signals for the formation of the MG-tMSH hemithioacetal as a function of time were consistent with the formation of the hemithioacetal. The resonances of the cysteine H-2 protons in the truncated mycothiol (region between 2.9–2.8 ppm) were clearly observed to alter over reaction time with MG. In the current experiment, the change in chemical shift of H-2 (δ 2.90–2.80 ppm) in tMSH and δ 3.00–2.80 in the MG-tMSH hemithioacetal) as well as additional splitting as a result of formation of diastereomeric MG adducts is consistent with the formation of the MG-tMSH hemithioacetal. This pattern became more defined after 15 min incubation. No significant change in NMR signals were observed after 30 min incubation (Figure S9).

Table S2 summarizes calculated versus experimental chemical shifts for tMSH and the MG-tMSH hemithioacetal. The estimated chemical shifts were calculated employing ChemBioDraw Ultra 12.0 software (<http://www.cambridgesoft.com>).

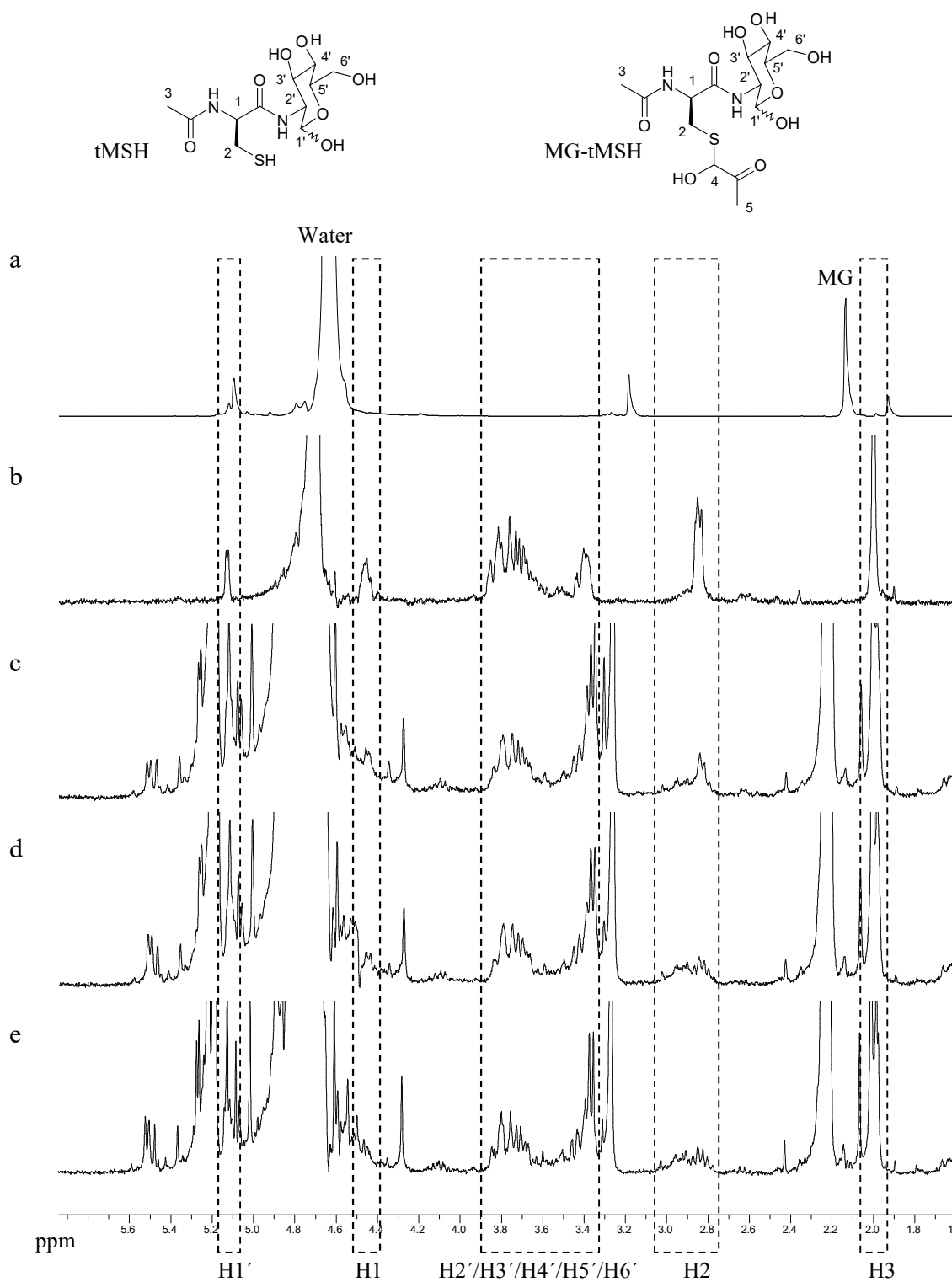


Figure S9. The ¹H NMR (300 MHz) spectra of various incubation times for the formation of the MG-tMSH hemithioacetal: (a) MG, (b) tMSH, (c) reaction incubated for 2 min, (d) reaction incubated for 15 min and (e) reaction incubated for 30 min.

Table S2. Summary of chemical shifts (CS) and integrations (int.) of NMR signal for MG-GSH equilibration time comparing to the signal of GSH (N/A = not available because the signal was obscured by water and MG peaks).



Peak	<i>tMSH</i>				<i>MG-tMSH</i>			
	[†] Predicted CS (ppm)	Actual CS (ppm)	Predicted int.	Actual int.	[†] Predicted CS (ppm)	Actual Cs (ppm)	Predict Int.	Actual int.
H1	4.39	4.50–4.43	1	0.93	4.37	5.51	1	1.37
H2	2.73–2.96	2.89–2.80	2	2.07	3.21	3.05–2.76	2	2.00
H3	2.06	2.00	3	3.00	2.06	2.04–1.96	3	9.37
H4	-	-	-	-	4.39	N/A	1	N/A
H5	-	-	-	-	2.19	2.35–2.24	3	8.73
H1'	4.88	5.14	1	0.61	4.88	N/A	1	N/A
H2'-H6'	3.52–4.16	3.89–3.35	6	7.15	3.52–4.16	3.89–3.23	6	22.55

[†]Chemical shifts are estimated by ChemBioDraw Ultra 12.0 (<http://www.cambridgesoft.com>) software.

Determination of the Hemithioacetal Dissociation Constant

The dissociation constant of the MG-GSH hemithioacetal has been previously derived for thiols reacting with MG [1-6] and can be calculated from the equation, $\Delta A_{240} = C[\text{MG}]_t / (K_d + [\text{MG}]_t)$, where ΔA_{240} is the net increase in absorbance at 240 nm after the reaction reaches its equilibrium and is read against a blank containing thiol, C is the total concentration of thiol multiplied by the collection of extinction coefficients of MG, tMSH and MG-tMSH ($(\epsilon_{\text{MG-tMSH}} - \epsilon_{\text{MG}} - \epsilon_{\text{tMSH}})[\text{tMSH}]_t$), $[\text{MG}]_t$ is the total concentration of MG and K_d is the dissociation constant. The dissociation constant can be determined from the plot of the change in A_{240} as a function of the concentration of MG.

The determination of the dissociation constant of the MG-tMSH hemithioacetal was performed using various concentrations of MG (0.5–100 mM), which were incubated with a fixed concentration of tMSH (0.2 mM) in 50 mM KPB (pH 6.6) for 30 min at room temperature (1 mL total). The increase in absorbance at 240 nm after the reaction reached its equilibrium (30 min, data from the previous experiment on hemithioacetal equilibrium time) was detected using a SpectraMax spectrophotometer. The investigation on the dissociation constant of MG-GSH under the same conditions was performed in parallel as a control. Even though K_d of MG-GSH was already reported, the experiment was repeated to confirm the accuracy of our experimental protocols [1-6]. However, in this case MG-GSH was incubated for 15 min to allow the reaction to reach its equilibrium. The dissociation profile of MG-GSH suggested its K_d of approx. 3.19 ± 0.29 mM (Figure S10A), which was in excellent agreement to the literature value (K_d of 3.1 mM).[1,2] The MG-tMSH dissociation profile suggested that the K_d of MG-tMSH was approx. 3.33 ± 0.41 mM (Figure S10B).

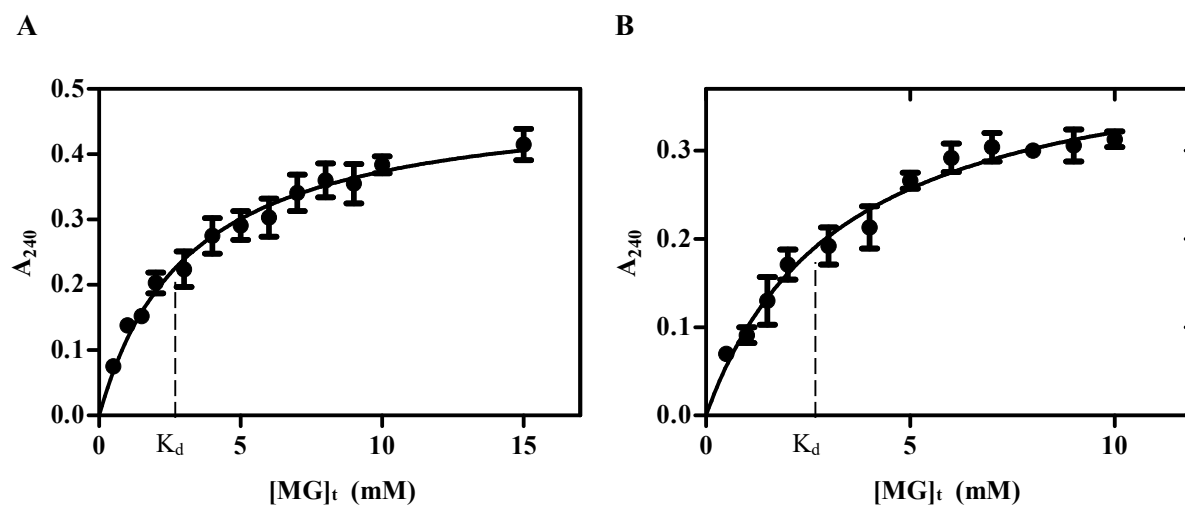


Figure S10. The determination of the dissociation constant (K_d) of (A) MG-GSH and (B) MG-tMSH. The experiments were performed in 50 mM KPB (pH 6.6) at room temperature. $[MG]_t$ is the total MG concentration from all species.

Assay Monitoring of the Thioester Product

The absorbance for monitoring of the Glo1 reaction was considered using Ni^{2+} -reconstituted PDO (4.5 μ g in 300 μ L assay) and the hemithioacetal (MG-tMSH) substrate (0.5 mM), in 50 mM KPB (pH 6.6). The substrate, MG-tMSH (K_d of 3.3 mM, data from previous experiment) was incubated for 30 min before mixing with the enzyme. The reactions were incubated at different time periods and the absorbance between 230–300 nm was scanned. The maximum absorbance to detect the formation of the product of the Glo1 reaction (*S*-D-lactoyl-des-*myo*-inositol mycothiol) was determined. Control experiments were performed using commercial yeast Glo1 (0.15 μ g in 300 μ L assay) with MG-GSH (0.1 mM, K_d of 3.1 mM) in 50 mM KPB (pH 6.6). MG-GSH was incubated for 15 min at room temperature before performing the enzymatic assay. Since the optimum absorbance for the product of the Glo1 reaction, *S*-D-lactoylglutathione, was already reported,[1,4,6,7] this experiment was repeated to confirm the accuracy of our protocols.

It has been previously reported that the increase in UV absorbance at 240 nm observed during the reaction of Glo1 is due to the formation of the product, *S*-D-lactoylglutathione, from the Glo1 reaction using MG-GSH as a substrate.[1,4,6] Our experiment on the monitoring of the Glo1 reaction using the commercial yeast Glo1 and MG-GSH suggested that the absorbance between 230–260 nm increases as a function of reaction time (data not shown). Thus, the absorbance at 240 nm was chosen for general Glo1 reaction kinetics studies since this wavelength could offer a more selective monitoring of the product from background contributions, which was especially the case when shorter wavelengths (below 240 nm) were used as interference from protein and peptide thiol that usually would occur.

The monitoring of the reaction kinetics of the PDO Glo1 reaction was similarly investigated. The wavelength scan of the PDO reaction using Ni^{2+} -reconstituted PDO with MG-tMSH indicated that there was only a slight change in intensity when the chosen wavelength to monitor the reaction was greater than 260 nm. Since tMSH is likely not the real substrate for the reaction, the difference between the wavelength scans for various time periods were small (data not shown). However, the monitored profiles at various wavelengths suggested that the detection of the product, *S*-D-lactoyl-des-*myo*-inositol mycothiol, at 240 nm offered the most defined signal. (Figure S11).

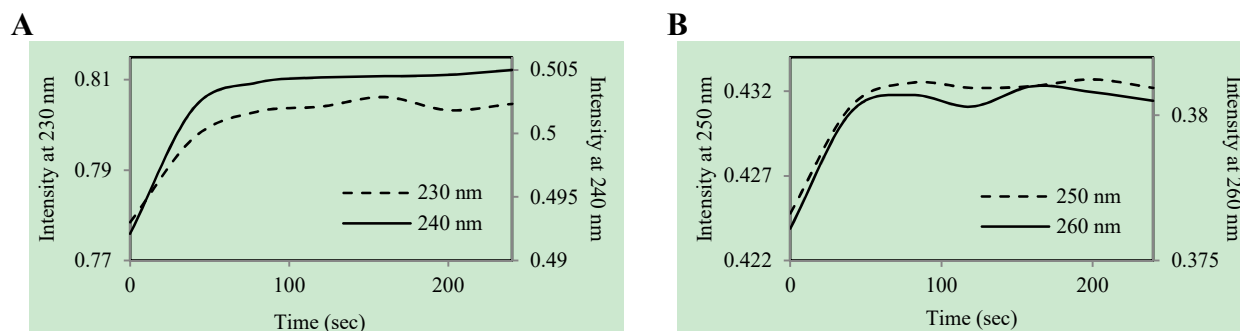


Figure 11. The UV detection of product thioester at specific wavelengths including (A) 230 and 240 nm and (B) 250 and 260 nm show the product formation from the reaction of Ni²⁺-reconstituted PDO (4.5 µg in 300 µL assay) using MG-tMSH (0.5 mM) as substrate in 50 mM KPB (pH 6.6).

Detection of the PDO Glo1 Reaction Product

The identification of the product from the PDO Glo1 reaction, *S*-D-lactoyl-des-*myo*-inositol mycothiol, was performed to confirm the enzymatic function of the putative enzymes. Apo-PDO (25 µg in 600 µL assay) was incubated with NiCl₂ (5 equivalents) overnight at 4 °C. The assay was performed using the substrate MG-tMSH (5 mM, *K_d* of 3.3 mM) in 50 mM KPB (pH 6.6) that had been incubated at room temperature for 30 min prior to assaying. The reaction was allowed to remain at room temperature for one hour. The product of the reaction was isolated by HPLC chromatography using a Waters µBandapak C18 reverse phase radial compression column (25 × 100 nm) and a flow rate of 1 mL/min with 1% increment of acetonitrile in water containing 0.1% TFA over a 100 min interval. The product was monitored at 280 nm and was identified by ESI-MS.

Comparison of the HPLC chromatograms (Figure S12) of the control experiments (MG, tMSH and the enzyme under the same concentrations as in the enzymatic reaction), indicated the formation of a new compound having a retention time (*t_R*) of 54 min. ESI-MS analysis of this isolated material was in agreement with the expected product therefore confirming that this peak contained the thioester product of the enzymatic reaction (Figure S13). Thus, this experiment is also consistent with PDO serving as a Glo1 enzyme.

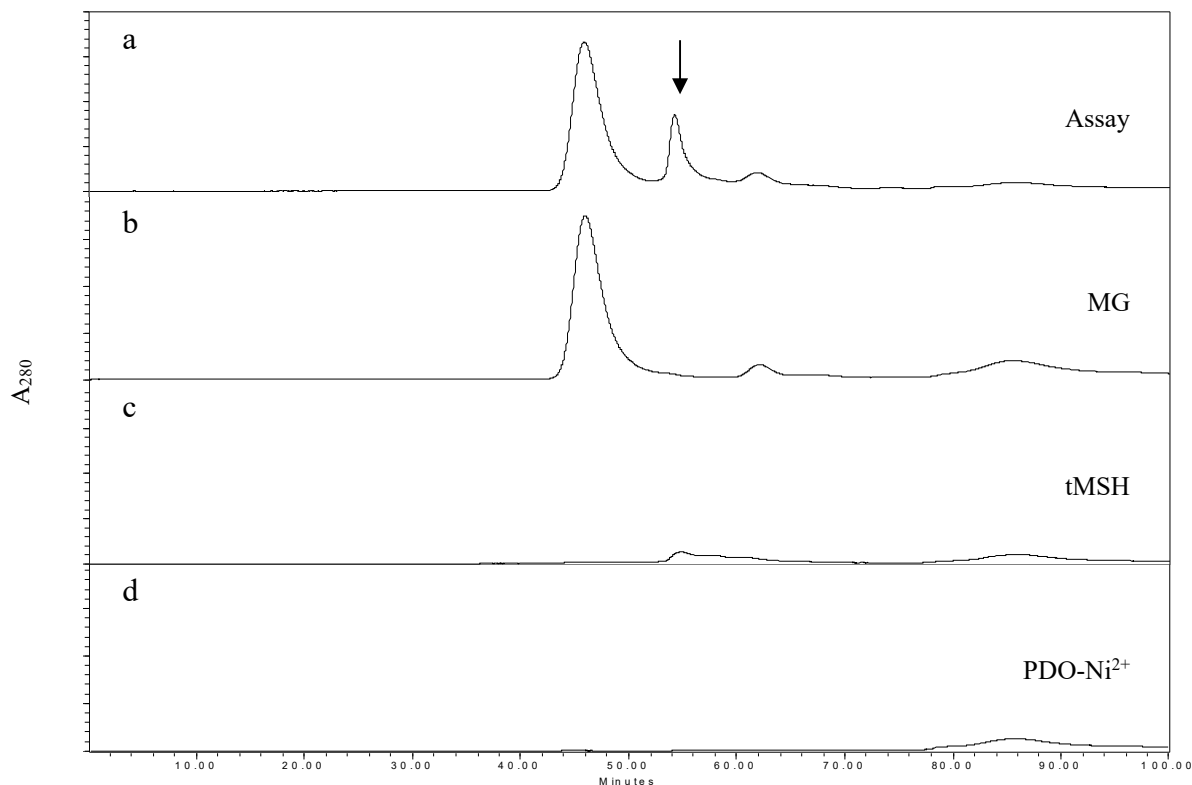


Figure S12. The reverse phase C18 HPLC chromatograms of (a) the assay reaction of Ni²⁺-reconstituted PDO (25 µg) and MG-tMSH (5 mM) compared to those of (b) MG, (c) tMSH and (d) Ni²⁺-reconstituted PDO that employed the same concentrations as in the reaction. The HPLC chromatograms were monitored at 280 nm and the product was eluted from the column using 1% increment of acetonitrile in water containing 0.1% TFA over 100 min interval with a flow rate of 1 mL/min. The eluted peak with *t_R* of 54 min contained the desired product (indicated by arrow) as confirmed by ESI-MS.

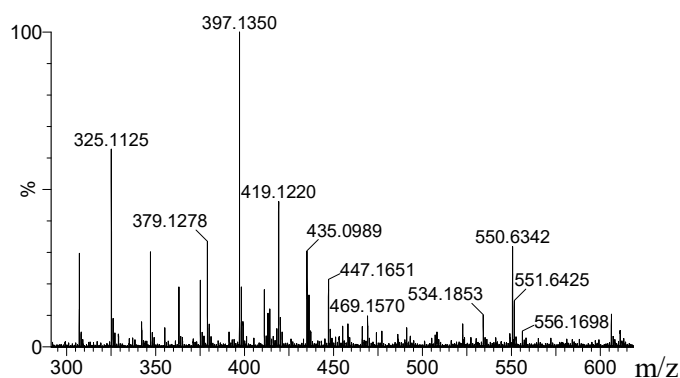


Figure S13. The electrospray mass spectrum of the HPLC isolated *S*-D-lactoyl-des-*myo*-inositol mycothiol exhibiting the expected the molecular mass of 397.1 Da (calculated MW of 396.4 Da). Other signals include *m/z* 325 (tMSH⁺, 60%), 379.1 (tMSHK⁺, 30%), 419.1 (Na⁺ adduct of *S*-D-lactoyl-des-*myo*-inositol mycothiol Na⁺, 50%) and 435.1 (K⁺ adduct of *S*-D-lactoyl-des-*myo*-inositol mycothiol, 30%). Masses at approximately 550 Da were from background.

Table S3. The calculation for the amount of metals contained in the “*as isolated*” PDO and PLA using ICP-MS analysis.

<i>Proteins</i>	<i>Metals</i>	<i>MW</i> <i>(g/mol)</i>	<i>1st [Metal]</i> <i>(mg/L)</i>	<i>2nd [Metal]</i> <i>(mg/L)</i>	<i>Ave.</i> <i>[metal]</i> <i>(mg/L)</i>	<i>[Metal]</i> <i>(μM)</i>	<i>[Metal]/[Protein]</i> <i>ratio</i>
PDO	Cobalt	58.93	0.006	0.006	0.006	2.04	0.019
	Copper	63.55	0.005	0.005	0.005	1.57	0.015
	Nickel	58.69	0.053	0.051	0.052	17.72	0.168
	Zinc	65.39	0.057	0.056	0.057	17.28	0.164
PLA	Copper	63.55	0.024	0.023	0.024	0.37	0.082
	Nickel	58.69	0.03	0.028	0.029	0.49	0.109
	Zinc	65.39	0.047	0.046	0.047	0.71	0.157

Table S4. Metal content of “as isolated” PDO (5.28 μ M) from *Streptomyces coelicolor* in Chelex-treated water as determined by ICP-MS. The experiment was performed in duplicate using Chelex-treated water as reference. The metals that have higher level of detection than those of the reference are highlight in grey.

<i>Metal analysis</i>	<i>Detection limit (mg/L)</i>	<i>Metal detection (mg/L) Trial 1</i>	<i>Metal detection (mg/L) Trial 2</i>	<i>Metal detection in Chelex-treated water (mg/L)</i>
Aluminum (Al)	0.01	<0.01	<0.01	<0.01
Antimony (Sb)	0.005	<0.005	<0.005	<0.005
Arsenic (As)	0.001	<0.001	<0.001	<0.001
Barium (Ba)	0.01	<0.01	<0.01	<0.01
Beryllium (Be)	0.001	<0.001	<0.001	<0.001
Bismuth (Bi)	0.001	<0.001	<0.001	<0.001
Boron (B)	0.05	<0.05	<0.05	<0.05
Cadmium (Cd)	0.0001	<0.0001	<0.0001	<0.0001
Calcium (Ca)	0.5	<0.5	<0.5	<0.5
Chromium (Cr)	0.001	<0.001	<0.001	<0.001
Cobalt (Co)	0.0005	0.0006	0.0006	<0.0005
Copper (Cu)	0.001	0.005	0.005	<0.001
Iron (Fe)	0.05	<0.05	<0.05	<0.05
Lead (Pb)	0.001	<0.001	<0.001	<0.001
Magnesium (Mg)	0.5	<0.5	<0.5	<0.5
Manganese (Mn)	0.001	<0.001	<0.001	<0.001
Molybdenum (Mo)	0.001	<0.001	<0.001	<0.001
Nickel (Ni)	0.002	0.053	0.051	<0.002
Phosphorus (P)	0.05	<0.05	<0.05	<0.05
Potassium (K)	1	<1	<1	<1
Selenium (Se)	0.005	<0.005	<0.005	<0.005
Silicon (Si)	0.1	<0.1	<0.1	<0.1
Silver (Ag)	0.0001	<0.0001	<0.0001	<0.0001
Sodium (Na)	0.5	<0.5	<0.5	<0.5
Strontium (Sr)	0.001	<0.001	<0.001	<0.001
Thallium (Tl)	0.0003	<0.0003	<0.0003	<0.0003
Tin (Sn)	0.001	<0.001	<0.001	<0.001
Titanium (Ti)	0.002	<0.002	<0.002	<0.002
Tungsten (W)	0.01	<0.01	<0.01	<0.01
Uranium (U)	0.005	<0.005	<0.005	<0.005
Vanadium (V)	0.001	<0.001	<0.001	<0.001
Zinc (Zn)	0.003	0.057	0.056	<0.003
Zirconium (Zr)	0.004	<0.004	<0.004	<0.004

Table S5. Metal content of “as isolated” PLA, (4.54 μ M) from *Streptomyces coelicolor* in Chelex-treated water as determined by ICP-MS. The experiment was performed in duplicate using Chelex-treated water as reference. The metals that have higher level of detection than those of the reference are highlight in grey.

<i>Metal analysis</i>	<i>Detection limit (mg/L)</i>	<i>Metal detection (mg/L) Trial 1</i>	<i>Metal detection (mg/L) Trial 2</i>	<i>Metal detection in Chelex-treated water (mg/L)</i>
Aluminum (Al)	0.01	<0.01	<0.01	<0.01
Antimony (Sb)	0.005	<0.005	<0.005	<0.005
Arsenic (As)	0.001	<0.001	<0.001	<0.001
Barium (Ba)	0.01	<0.01	<0.01	<0.01
Beryllium (Be)	0.001	<0.001	<0.001	<0.001
Bismuth (Bi)	0.001	<0.001	<0.001	<0.001
Boron (B)	0.05	<0.05	<0.05	<0.05
Cadmium (Cd)	0.0001	0.0002	0.0002	<0.0001
Calcium (Ca)	0.5	<0.5	<0.5	<0.5
Chromium (Cr)	0.001	<0.001	<0.001	<0.001
Cobalt (Co)	0.0005	<0.0005	<0.0005	<0.0005
Copper (Cu)	0.001	0.024	0.023	<0.001
Iron (Fe)	0.05	<0.05	<0.05	<0.05
Lead (Pb)	0.001	0.003	0.003	<0.001
Magnesium (Mg)	0.5	<0.5	<0.5	<0.5
Manganese (Mn)	0.001	<0.001	<0.001	<0.001
Molybdenum (Mo)	0.001	<0.001	<0.001	<0.001
Nickel (Ni)	0.002	0.03	0.028	<0.002
Phosphorus (P)	0.05	<0.05	<0.05	<0.05
Potassium (K)	1	<1	<1	<1
Selenium (Se)	0.005	<0.005	<0.005	<0.005
Silicon (Si)	0.1	<0.1	<0.1	<0.1
Silver (Ag)	0.0001	0.0006	0.0005	<0.0001
Sodium (Na)	0.5	2.4	2.4	2.1
Strontium (Sr)	0.001	<0.001	<0.001	<0.001
Thallium (Tl)	0.0003	<0.0003	<0.0003	<0.0003
Tin (Sn)	0.001	<0.001	<0.001	<0.001
Titanium (Ti)	0.002	<0.002	<0.002	<0.002
Tungsten (W)	0.01	<0.01	<0.01	<0.01
Uranium (U)	0.005	<0.005	<0.005	<0.005
Vanadium (V)	0.001	<0.001	<0.001	<0.001
Zinc (Zn)	0.003	0.047	0.046	<0.003
Zirconium (Zr)	0.004	<0.004	<0.004	<0.004

References

1. Vander Jagt, D.L.; Han, L.P.; Lehman, C.H. Kinetic evaluation of substrate specificity in the glyoxalase-I-catalyzed disproportionation of α -ketoaldehydes. *Biochemistry* **1972**, *11*, 3735-3740.
2. Vince, R.; Daluge, S.; Wadd, W.B. Studies on the inhibition of glyoxalase I by S-substituted glutathiones. *J. Med. Chem.* **1971**, *14*, 402-404.
3. Cliffe, E.E.; Waley, S.G. The mechanism of the glyoxalase I reaction, and the effect of ophthalmic acid as an inhibitor. *Biochem. J.* **1961**, *79*, 475-482.
4. Creighton, D.J.; Migliorini, M.; Pourmotabbed, T.; Guha, M.K. Optimization of efficiency in the glyoxalase pathway. *Biochemistry* **1988**, *27*, 7376-7384.
5. Griffis, C.E.; Ong, L.H.; Buettner, L.; Creighton, D.J. Nonstereospecific substrate usage by glyoxalase I. *Biochemistry* **1983**, *22*, 2945-2951.
6. Vander Jagt, D.L.; Daub, E.; Krohn, J.A.; Han, L.P. Effects of pH and thiols on the kinetics of yeast glyoxalase I. An evaluation of the random pathway mechanism. *Biochemistry* **1975**, *14*, 3669-3675.
7. Clugston, S.L.; Barnard, J.F.; Kinach, R.; Miedema, D.; Ruman, R.; Daub, E.; Honek, J.F. Overproduction and characterization of a dimeric non-zinc glyoxalase I from *Escherichia coli*: evidence for optimal activation by nickel ions. *Biochemistry* **1998**, *37*, 8754-8763.
8. Rae, C.; O'Donoghue, S.I.; Bubb, W.A.; Kuchel, P.W. Stereospecificity of substrate usage by glyoxalase I: nuclear magnetic resonance studies of kinetics and hemithioacetal substrate conformation. *Biochemistry* **1994**, *33*, 3548-3559.